GDCh Research Article Angewandte International Edition Chemie www.angewandte.org

How to cite: *Angew. Chem. Int. Ed.* **2025**, e21100
doi.org/10.1002/anie.202521100

Photochemistry

Copper-Catalyzed Phosphorus Radical Transformations for the Assembly of P-Stereogenic Architectures

*Yujin Zi[+], Boxuan Yang[+], Ziqi Ye, Yu-Mei Lin, Qianyi Zhao, Binju Wang, and Lei Gong**

Abstract: Phosphorus-centered radicals hold transformative potential for organophosphorus synthesis, yet their configurational lability and distinctive reactivity profiles have historically restricted their application in asymmetric catalysis. Herein, we report a copper-photoredox catalytic system that enables the stereoselective generation of copper-bound P-centered radicals and their subequent stereoretentive transformations within a well-defined chiral environment. The synergistic approach achieves unprecedented kinetic resolutions of racemic H-phosphinates with α-trifluoromethyl styrenes or *gem*-difluorostyrenes, delivering 85 fluorine-containing P-chiral phosphinates with up to 98% ee. The method thereby bridges a synthetic gap for these previously inaccessible, pharmacologically significant compounds. Mechanistic and computational studies reveal a stereochemical relay: enantiodiscriminatory binding of racemic substrates, photoinduced ligand-to-metal charge transfer (LMCT) for radical generation, and stereoretentive bond formation. By reconciling radical reactivity with stereochemical fidelity, our strategy establishes metallaphotoredox catalysis as a versatile paradigm for heteroatom-centered stereochemistry.

Introduction

Radical chemistry has emerged as a powerful strategy for chemical bond formation, offering distinct and complementary advantages over conventional ionic processes.[1–9] These include unique reactivity patterns, operationally mild reaction conditions, high chemoselectivity, and broad functional group tolerance.[10–15] The rapid development of photocatalysis and electrocatalysis has further underscored the significance of radical-based transformations in modern synthetic chemistry.[16–22] However, achieving asymmetric synthesis through radical intermediates, particularly via stereoretentive pathways that preserve chirality through transient open-shell species, remains a formidable challenge.[23–25] Recent advances in transition metal catalysis and enzyme catalysis have partially addressed limitations in carbon-centered radicals.[26–30] For example, Baran et al. employed tethered nickel species to stabilize transient carbon radicals derived from sulfonylhydrazides, facilitating stereoretentive C—C couplings.[31] Liu et al. developed a copper-catalyzed asymmetric amination of prochiral alkyl radicals using precisely engineered chiral anionic *N*,*N*,*P*-ligands.[32] Melchiorre et al. reported a non-natural photodecarboxylase capable of promoting stereospecific radical cross-coupling between α,β-unsaturated aldehydes and carboxylic acids.[33] These approaches exploit precise molecular organization and tailored environments to control carbon radical stereochemistry. However, progress in phosphorus-centered radical chemistry is notably scarce.

Stereochemical manipulation of phosphorus-centered radicals poses substantial thermodynamic and kinetic obstacles.[34] P-chiral organophosphorus radicals exhibit remarkably low inversion barriers (e.g., $\Delta G^{\neq} \approx 12$ kcal mol^{-1} for Ph^{t}BuP(=O)•) and distinctive reactivity profiles, making them prone to rapid racemization and competing processes such as self-couplings and α-/β-scission. These factors often outcompete stereoselective bond formation, creating significant barriers for asymmetric synthesis.[35] This challenge is particularly pertinent given the growing pharmaceutical interest in P-stereogenic molecules.[36–40] Fluorinated P-chiral architectures, for instance, combine the stereoelectronic effects of phosphorus chirality with the enhanced metabolic stability and ligand–receptor binding specificity afforded by fluorine substitution (Scheme 1a).[41,42] Sofosbuvir exemplifies this class, where fluorination directly improves pharmacological properties. Despite their potential, effective synthetic strategies remain limited due to the need to simultaneously achieve precise stereocontrol, compatibility with fluorinated building blocks, and broad functional group tolerance.

Building on our previous work in photochemical asymmetric synthesis[43–49] and recent advances in metalloradical-based stereoselective transformations,[50–55] we conceive a dual catalytic paradigm to tackle current challenges. Our

[*] Y. Zi[+], B. Yang[+], Z. Ye, Prof. Dr. Y.-M. Lin, Prof. Dr. B. Wang, Prof. Dr. L. Gong
College of Chemistry and Chemical Engineering, Xiamen University, Xiamen 361005, China
E-mail: gongl@xmu.edu.cn
Dr. Q. Zhao
School of Chemistry and Chemical Engineering, Henan Normal University, Xinxiang, China
Prof. Dr. L. Gong
Innovation Laboratory for Sciences and Technologies of Energy Materials of Fujian Province (IKKEM), Xiamen, China
[+] Both authors contributed equally to this work.

Additional supporting information can be found online in the Supporting Information section

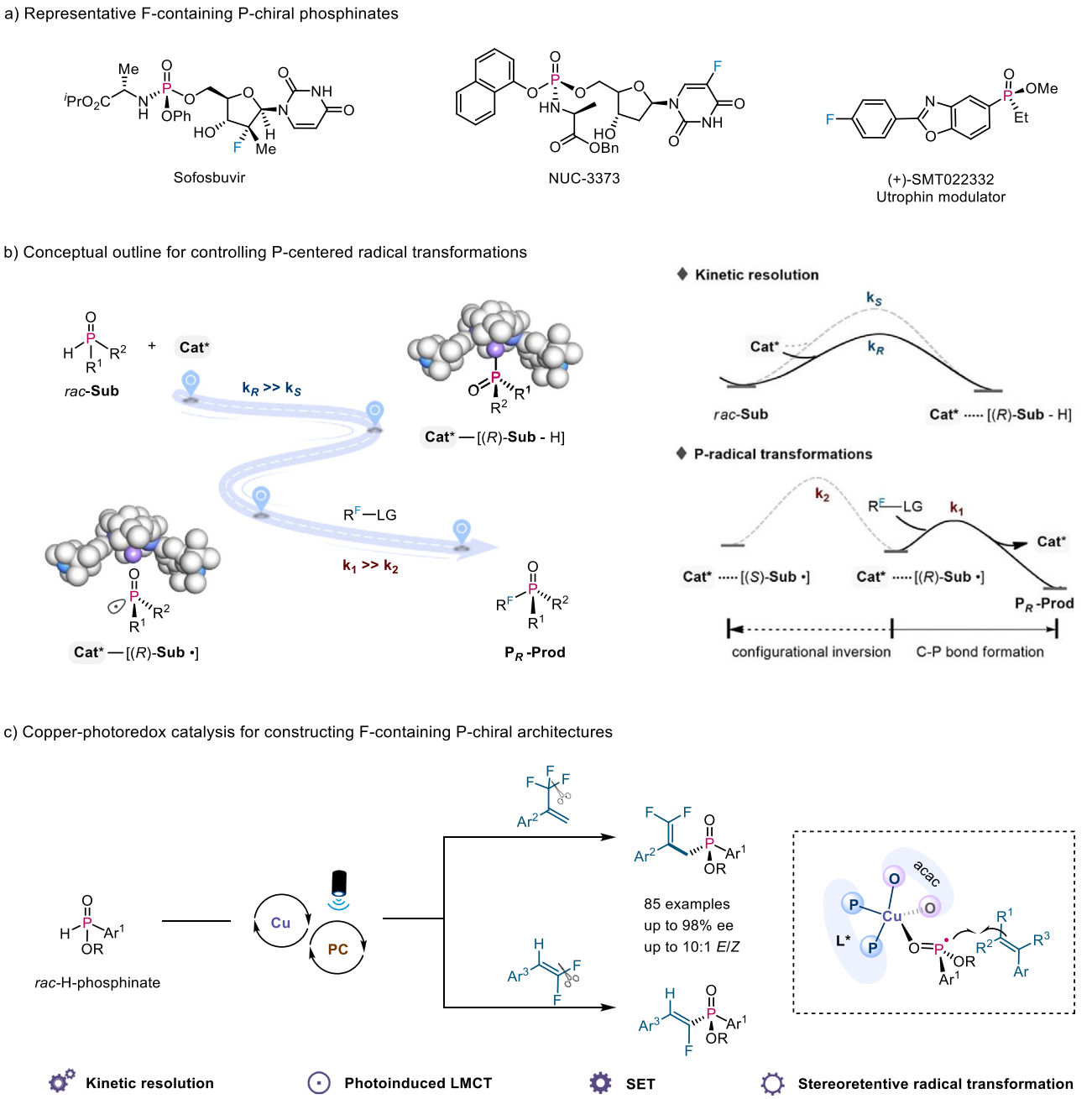

Scheme 1. Overview of this work.

approach hinges on the hypothesis that light-induced generation of chiral P-radicals bound to a metal center within a well-defined chiral environment could enable stereoretentive transformations prior to configurational inversion ($k_1 >> k_2$, Scheme 1b). Guided by this principle, we established a noble-metal-free catalytic platform synergizing a sterically demanding chiral diphosphine-copper catalyst and 1,2,3,5-tetrakis(carbazol-9-yl)-4,6-dicyanobenzene (4CzIPN) as the photoredox catalyst. The system enables the first visible light-triggered kinetic resolution of H-phosphinates under ambient conditions, employing α-trifluoromethyl styrenes or *gem*-difluorostyrenes as coupling partners (Scheme 1c). It provides efficient access to a broad array of fluorine-containing P-chiral phosphinates (85 examples, up to 98% ee), encompassing structures relevant to drug discovery and bioactive molecule development.

Results and Discussion

Reaction Optimization

Capitalizing on the synthetic versatility of α-trifluoromethyl alkenes as fluorinated building blocks, we chose 1-methyl-4-(3,3,3-trifluoroprop-1-en-2-yl)benzene (**2a**) as the model coupling partner for the photochemical reaction of racemic

Table 1: Reaction optimization.

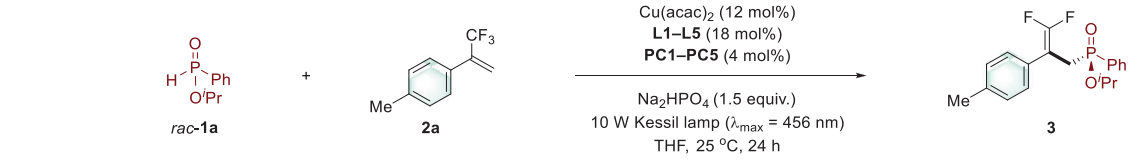

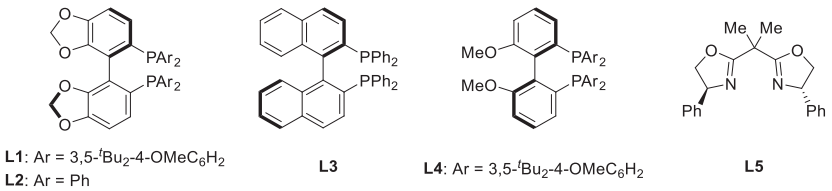

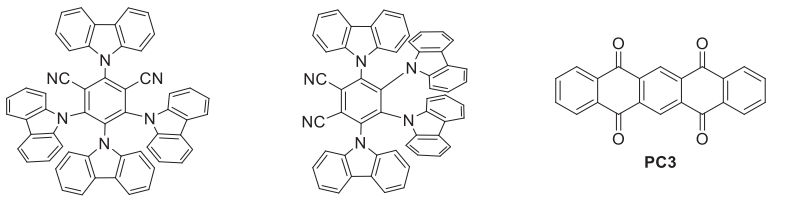

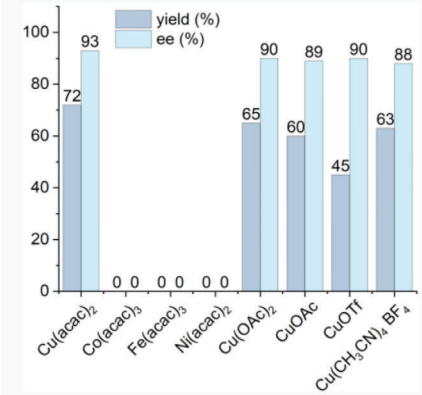

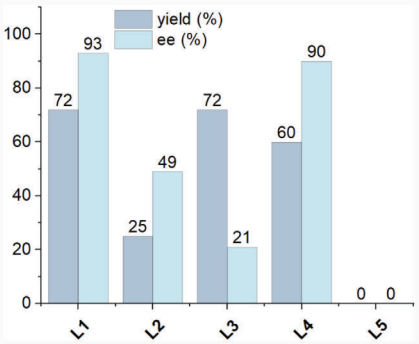

Entry	Variations from standard conditions[a]	Yield of 3 (%)[b]	Ee of 3 (%)[c]
1	None	72	93
2	**PC2** instead of **PC1**	68	84
3	**PC3** instead of **PC1**	0	n.a.
4	**PC4** instead of **PC1**	65	90
5	**PC5** instead of **PC1**	0	n.a.
6	In the absence of light irradiation	0	n.a.
7	In the absence of the photocatalyst	0	n.a.
8	In the absence of $Cu(acac)_2$ and **L1**	0	n.a.
9	In the absence of **L1**	8	n.d.
10	Air instead of argon	0	n.a.

[a] Reaction conditions: *rac*-**1a** (0.40 mmol), **2a** (0.10 mmol), metal salt (0.012 mmol), chiral ligand (**L1**–**L5**, 0.018 mmol), photocatalyst (**PC1**–**PC5**, 0.0040 mmol), Na_2HPO_4 (0.15 mmol), THF (1.0 mL), 25 °C, under argon. For further details on the screening of solvents, please refer to the Supporting Information. [b] Isolated yield. [c] Ee value determined by chiral HPLC. N.d. = not detected, n.a. = not applicable.

isopropyl phenylphosphinate (*rac*-**1a**). Initial reactions were conducted using a 4:1 molar ratio of *rac*-**1a** to **2a** to ensure high conversion. Following a systematic exploration of reaction conditions (see the Supporting Information for details), we identified that irradiating *rac*-**1a** and **2a** in the presence of $Cu(acac)_2$ (12 mol%, acac = acetylacetonate), a sterically demanding chiral diphosphine ligand ((*R*)-DTBM-SEGPHOS, **L1**, 18 mol%), 4CzIPN (**PC1**, 4 mol%), and Na_2HPO_4 (1.5 equiv.) in THF under a 10 W Kessil lamp (λ_{max} = 456 nm) afforded the desired tertiary phosphinate (**3**) in 72% yield and 93% ee (Table 1, entry 1). Alternative 3d transition metal acetylacetonates, such as $Co(acac)_3$, $Fe(acac)_3$, and $Ni(acac)_2$, failed to produce the target product. Conversely, other copper salts like $Cu(OAc)_2$, CuOAc, CuOTf, and $Cu(CH_3CN)_4BF_4$ displayed slightly reduced enantioselectivity (88%–90% ee) and lower yields (45%–65%). Chiral diphosphine ligands with less steric bulk (**L2**–**L4**) proved less effective and selective, while a bisoxazoline ligand (**L5**) rendered the reaction unfeasible (right image). Among the tested photocatalysts, including 3,4,5,6-tetrakis(carbazol-9-yl)-1,2-dicyanobenzene (4CzPN, **PC2**), 5,7,12,14-pentacenetetrone (**PC3**), $Ir[dF(CF_3)ppy]_2(dtbbpy)PF_6$ (**PC4**), and *fac*-$Ir(ppy)_3$ (**PC5**), **PC1** consistently delivered superior yield and enantioselectivity (entries 2–5). Control experiments underscored the necessity of light irradiation, photocatalyst, copper salt, chiral ligand, and an inert atmosphere for the transformation (entries 6–10). Remarkably, the removal of the chiral ligand led to a dramatic decline in yield to a mere 8%, highlighting a ligand-accelerated reaction process (entry 9).

Substrate Scope for the Photochemical C(sp^3)—P Formation Reaction

With the optimized conditions established, we systematically explored the substrate scope of this photochemical C(sp^3)—P formation process (Scheme 2). Initial studies focused on α-trifluoromethyl styrene derivatives, where substituent positions on the phenyl ring were found to significantly influence

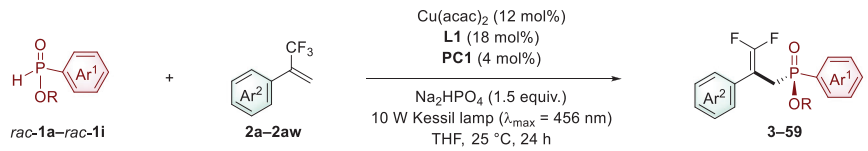

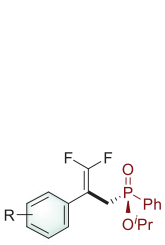

3, R = 4-Me, 72% yield, 93% ee
4, R = 3-Me, 56% yield, 98% ee
5, R = 2-Me, 0% yield
6, R = H, 58% yield, 90% ee[a)]
7, R = 4-*n*-Pent, 63% yield, 92% ee
8, R = 4-^{i}Pr, 70% yield, 93% ee
9, R = 4-^{t}Bu, 64% yield, 92% ee
10, R = 4-TMS, 76% yield, 94% ee
11, R = 4-OH, 64% yield, 92% ee
12, R = 4-SMe, 64% yield, 94% ee
13, R = 4-OMe, 73% yield, 95% ee
14, R = 4-OPh, 71% yield, 93% ee
15, R = 4-OBn, 72% yield, 93% ee
16, R = 4-O^{t}Bu, 75% yield, 90% ee
17, R = 4-OCF_3, 57% yield, 93% ee

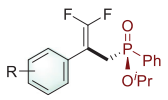

18, R = 4-CO_2Me, 62% yield, 93% ee
19, R = 3-CO_2Me, 56% yield, 92% ee
20, R = 4-CO_2Et, 62% yield, 93% ee
21, R = 4-CN, 64% yield, 91% ee
22, R = 4-SO_2Me, 63% yield, 91% ee
23, R = 4-Cl, 68% yield, 90% ee
24, R = 4-Br, 65% yield, 93% ee
25, R = 4-CF_3, 68% yield, 91% ee

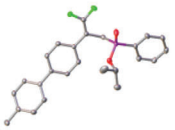

X-ray structure of **27**
(CCDC 2361292)

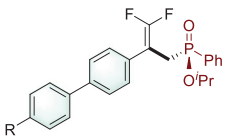

26, R = H, 83% yield, 95% ee
27, R = Me, 72% yield, 95% ee
28, R = *n*-Pent, 68% yield, 93% ee
29, R = Cl, 75% yield, 93% ee
30, R = Br, 69% yield, 95% ee
31, R = CO_2Me, 68% yield, 93% ee
32, R = CN, 72% yield, 94% ee
33, R = 2-naphthyl, 74% yield, 95% ee

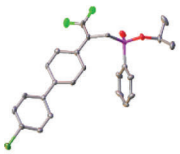

X-ray structure of **30**
(CCDC 2309605)

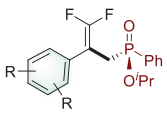

34, R = 3,5-di-Me, 67% yield, 93% ee
35, R = 3,5-di-Ph, 76% yield, 97% ee
36, R = 3,4-di-OMe, 68% yield, 93% ee
37, R = 3,5-di-OMe, 72% yield, 93% ee

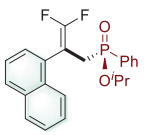

38, 61% yield, 93% ee

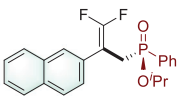

39, 75% yield, 94% ee

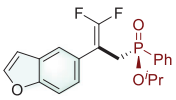

40, 61% yield, 95% ee

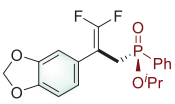

41, 68% yield, 94% ee

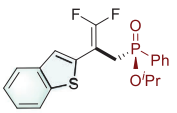

42, 55% yield, 94% ee

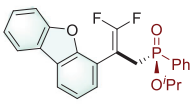

43, 71% yield, 93% ee

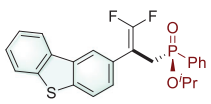

44, 69% yield, 92% ee

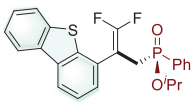

45, 72% yield, 92% ee

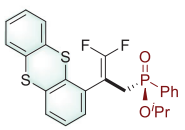

46, 71% yield, 94% ee

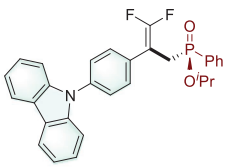

47, 75% yield, 92% ee

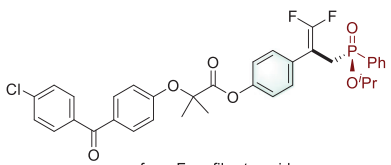

from Fenofibrate acid
48, 64% yield, 92% ee

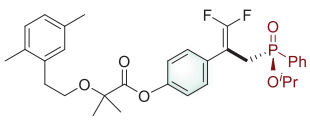

from Gemfibrozil
49, 60% yield, 94% ee

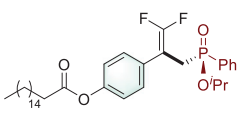

from Hexadecane acid
50, 59% yield, 98% ee

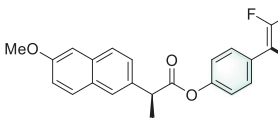

from Naproxen
51, 60% yield, >20:1 dr

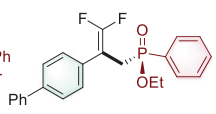

52, 81% yield, 83% ee

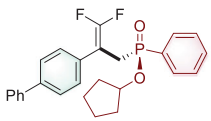

53, 72% yield, 86% ee

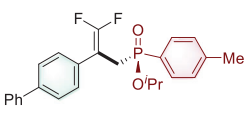

54, 72% yield, 92% ee

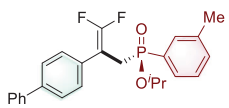

55, 63% yield, 95% ee

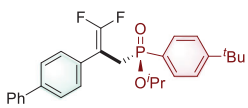

56, 71% yield, 94% ee

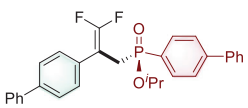

57, 72% yield, 90% ee

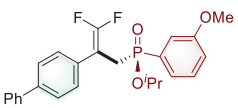

58, 75% yield, 92% ee

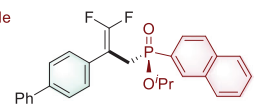

59, 70% yield, 90% ee

Scheme 2. Substrate scope for the photochemical reaction between racemic H-phosphinates and α-trifluoromethyl styrenes. Standard conditions: *rac*-**1a**–*rac*-**1i** (0.80 mmol), **2a**–**2aw** (0.20 mmol), $Cu(acac)_2$ (0.024 mmol), **L1** (0.036 mmol), **PC1** (0.0080 mmol), Na_2HPO_4 (0.30 mmol), THF (2.0 mL), 25 °C, under argon. [a)] Using 0.048 mmol of **L1**, rather than 0.036 mmol.

reaction outcomes. For example, shifting a methyl group from the *para*-position (product **3**, 72% yield) to the *meta*- (product **4**, 56% yield) and *ortho*- positions (product **5**, 0% yield) led to progressively lower yields. The unsubstituted analog yielded product **6** with 58% yield and 90% ee.

A wide range of *para*-substituted electron-donating groups, including *n*-pentyl (product **7**), isopropyl (product **8**), *t*-butyl (product **9**), trimethylsilyl (product **10**), hydroxyl (product **11**), methylthio (product **12**), methoxy (product **13**), phenoxy (product **14**), benzyloxy (product **15**), *t*-butoxy (product **16**), and trifluoromethoxy (product **17**), were well-tolerated, delivering yields of 57%–76% and enantioselectivity of 90%–95% ee. Similarly, substrates bearing electron-withdrawing substituents, such as methoxycarbonyl (products **18**, **19**), ethoxycarbonyl (product **20**), cyano (product **21**), methylsulfonyl (product **22**), chloro (product **23**), bromo (product **24**), and trifluoromethyl (product **25**), produced yields of 56%–68% and enantioselectivities of 90%–93% ee.

The method also accommodated 4-aryl-substituted (products **26**–**33**), disubstituted (products **34**–**37**), fused rings (products **38**, **39**), and heterocycle substrates (products **40**–**47**), all affording high enantioselectivity (92%–97% ee) and yields (55%–83%). X-ray crystallography confirmed the *R* configurations of products **27** (CCDC No. 2361292) and **30** (CCDC No. 2309605).[56] Importantly, the protocol was applicable to complex molecular frameworks derived from bioactive molecules, such as Fenofibrate acid (product **48**), Gemfibrozil (product **49**), and Hexadecane acid (product **50**), yielding products with 59%–64% and 92%–98% ee. A Naproxen-derived substrate (product **51**) delivered 60% with > 20:1 dr, further highlighting the method's synthetic utility.

Regarding racemic H-phosphinate substrates, ethyl (product **52**) and cyclopentyl phenylphosphinate (product **53**) showed somewhat diminished enantioselectivity (83% and 86% ee, respectively), underscoring the impact of the phosphate ester moiety. In contrast, phenyl-substituted variants, including 4-methyl (product **54**), 3-methyl (product **55**), 4-*t*-butyl (product **56**), 4-phenyl (product **57**), 3-methoxy (product **58**), and 2-naphthyl (product **59**) maintained consistently high performance (63%–75% yield, 90%–95% ee).

Extension to Photochemical C(sp^2)—P Formation

To expand the applicability of our copper-photoredox catalyzed kinetic resolution strategy, we explored the reactivity of racemic H-phosphinates with various fluorinated precursors. While asymmetric C(sp^2)—P cross-coupling of phosphine precursors with vinyl halides offers direct access to alkenylated P-stereogenic compounds with broad pharmaceutical applications, their development has been impeded by challenges in stereocontrol during P—C=C bond formation.[57–59] Our investigation revealed that this transformation could be successfully achieved via a copper-catalyzed photochemical process employing racemic H-phosphinates and *gem*-difluorostyrenes (Scheme 3).

Following systematic optimization, the ideal conditions were identified as follows: $Cu(acac)_2$ (10 mol%) as the copper source, chiral diphosphine ligand **L1** (18 mol%), 4CzIPN (**PC1**, 2 mol%) as the photocatalyst, 4 Å MS (20.0 mg) as the additive, in acetone under an argon atmosphere. Irradiation of racemic isopropyl phenylphosphinate (*rac*-**1a**) and methyl 4-(2,2-difluorovinyl)benzoate (**3a**) with a 10 W Kessil lamp (λ_{max} = 456 nm) provided the best outcomes (see the Supporting Information for details). This protocol yielded the monofluoroalkenylated phosphinate product (**60**) in 71% yield with an excellent *E:Z* ratio of 7:1 and 91% ee for the major *E*-isomer. X-ray crystallography confirmed its *S* configuration (CCDC No. 2440675).[56]

The protocol demonstrated broad generality across diverse *gem*-difluorostyrenes. (2,2-difluorovinyl)benzene derivatives bearing either electron-donating (products **61**–**66**) or electron-withdrawing groups (products **67**–**74**) on the phenyl ring delivered consistent results, with yields ranging from 53% to 69%, *E:Z* ratios of 3:1 to 7:1, and high enantioselectivity (85%–91% ee). Complex structures including fused rings (product **75**), disubstituted aryls (products **76**–**82**), heterocycles (products **83**, **84**), and drug-like fragments (products **85**–**88**) were also compatible, yielding 56%–70% with high selectivity (*E:Z* = 2.5:1–10:1, 80%–92% ee).

Enhanced Kinetic Resolution for H-Phosphinate Recovery

Leveraging the high energy barrier for enantiomer interconversion in H-phosphinate precursors, we next developed an efficient kinetic resolution procedure that enables the simultaneous formation of P-chiral tertiary phosphinates and recovery of enantioenriched starting materials (Scheme 4). Systematic investigations on reaction parameters for the photochemical resolution of *rac*-isopropyl phenylphosphinate (*rac*-**1a**) with 4-(3,3,3-trifluoroprop-1-en-2-yl)-1,1′-biphenyl (**2x**) identified the following optimal conditions: *rac*-**1a** (1.0 equiv.), **2x** (2.0 equiv.), $Cu(acac)_2$ (12 mol%), **L1** (24 mol%), **PC1** (4 mol%), and Na_2HPO_4 (1.5 equiv.) in THF under a 10 W blue LED irradiation (λ_{max} = 460 nm) at 10 °C for 48 h. Product (*R*)-**26** was obtained in 42% yield with 91% ee, while (*S*)-**1a** was recovered in 54% yield with 84% ee, corresponding to a selectivity factor (*s*) of 56. This KR protocol was successfully applied to a range of substrates. Reactions of *rac*-**1a** with various α-trifluoromethyl styrene derivatives, conducted under either identical or slightly altered conditions over 40−64 h, produced *gem*-difluoroallyl P-chiral phosphinate products (**13**–**15**, **27**–**32**, **35**, **39**, **41**, and **47**) with 39%–41% yield and 87%–91% ee. Concomitantly, (*S*)-**1a** was recovered in 51%–58% yield and 80%–90% ee, achieving *s* factors ranging from 42 to 55. These results underscore the robustness and efficiency of the method in enabling both asymmetric synthesis and high-fidelity substrate recovery.

Mechanistic Studies

To elucidate the reaction mechanism, a series of control experiments and spectroscopy analyses were

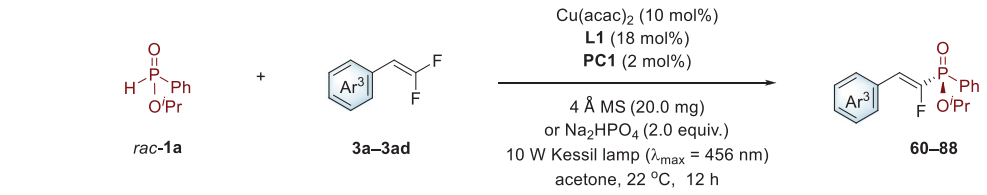

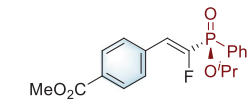

60, *E*:*Z* = 7:1, 71% yield, 91% ee

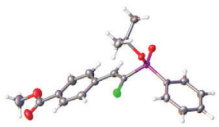

X-ray structure of **60**
(CCDC 2440675)

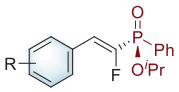

61, R = 4-H, *E*:*Z* = 5:1, 56% yield, 85% ee[a]
62, R = 4-Me, *E*:*Z* = 5:1, 67% yield, 90% ee[a]
63, R = 3-Me, *E*:*Z* = 6:1, 60% yield, 90% ee[a]
64, R = 4-^{i}Pr, *E*:*Z* = 5:1, 69% yield, 91% ee[a]
65, R = 4-^{t}Bu, *E*:*Z* = 5:1, 68% yield, 91% ee[a]
66, R = 4-OPh, *E*:*Z* = 4:1, 60% yield, 90% ee

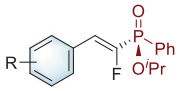

67, R= 4-Ph, *E*:*Z* = 3:1, 61% yield, 90% ee[a]
68, R= 3-Ph, *E*:*Z* = 5:1, 58% yield, 90% ee[a]
69, R = 4-F, *E*:*Z* = 6:1, 53% yield, 91% ee[a]
70, R = 4-Cl, *E*:*Z* = 5:1, 60% yield, 90% ee[a]
71, R = 4-Br, *E*:*Z* = 5:1, 67% yield, 87% ee[a]
72, R = 4-CF_3, *E*:*Z* = 5:1, 58% yield, 90% ee[a]
73, R = 4-CN, *E*:*Z* = 5:1, 62% yield, 90% ee[a]
74, R = 3-CO_2Me, *E*:*Z* = 7:1, 62% yield, 88% ee

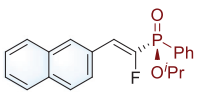

75, *E*:*Z* = 2.5:1
67% yield, 92% ee[a]

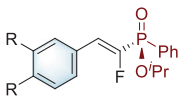

76, R = Me, *E*:*Z* = 5:1
68% yield, 90% ee[a]
77, R = Cl, *E*:*Z* = 5:1
69% yield, 90% ee[a]

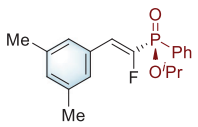

78, *E*:*Z* = 4:1
67% yield, 90% ee[a]

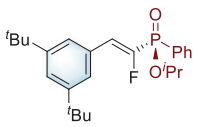

79, *E*:*Z* = 4:1
65% yield, 84% ee[a]

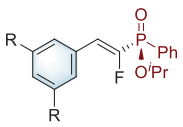

80, R = Cl, *E*:*Z* = 4:1, 62% yield, 90% ee[a]
81, R = Br, *E*:*Z* = 4:1, 70% yield, 86% ee[a]

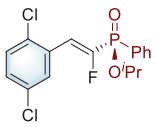

82, *E*:*Z* = 6:1
58% yield, 90% ee[a]

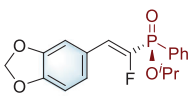

83, *E*:*Z* = 4:1, 60% yield, 90% ee

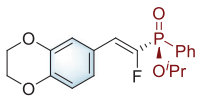

84, *E*:*Z* = 4:1, 56% yield, 80% ee

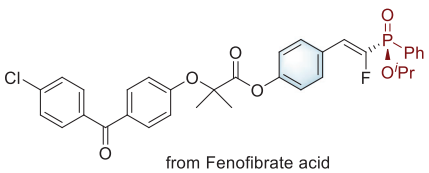

from Fenofibrate acid
85, *E*:*Z* = 6:1, 69% yield, 85% ee[b]

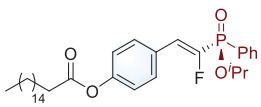

from Hexadecane acid
86, *E*:*Z* = 10:1, 66% yield, 90% ee

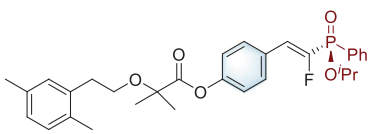

from Gemfibrozil
87, *E*:*Z* = 6:1, 68% yield, 86% ee[b]

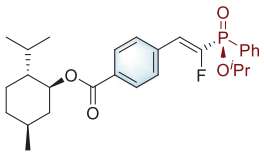

from *L*-Menthol
88, *E*:*Z* = 9:1, 66% yield, >20:1 dr

Scheme 3. Expanding our strategy to photochemical asymmetric C(sp^2)—P cross-coupling between racemic H-phosphinates and *gem*-difluorostyrenes. Standard conditions: *rac*-**1a** (0.30 mmol), **3a-3ad** (0.10 mmol), $Cu(acac)_2$ (0.010 mmol), **L1** (0.018 mmol), **PC1** (0.0020 mmol), 4 Å MS (20.0 mg), acetone (1.0 mL), 22 °C, under argon. [a] Using 0.20 mmol of Na_2HPO_4 (28.4 mg). [b] Using THF (1.0 mL), 15 h.

carried out (Scheme 5). Initially, the addition of 2,2,6,6 tetramethylpiperidine-1-oxyl (TEMPO, 5.0 equiv.) to the standard reaction between *rac*-**1a** and **2x** completely suppressed the formation of product **26**. High-resolution mass spectrometry (HRMS) analysis confirmed the presence of TEMPO-coupled byproducts, suggesting the involvement of radical intermediates.[60] Similarly, when a competitive radical acceptor, such as ethyl ((2-phenylallyl)sulfonyl)benzene, was introduced into the reaction, the formation of **26** was inhibited. Instead, HRMS analysis unveiled the generation of an alternative adduct, ethyl 2-((isopropoxy(phenyl)phosphoryl)methyl)acrylate (refer to the Supporting Information for more details), further supporting a radical-mediated pathway.

Electron paramagnetic resonance (EPR) spectroscopy provided direct evidence for the participation of P-centered radicals in the reaction. When 5,5-dimethyl-1-pyrroline *N*-oxide (DMPO) was introduced into the standard reaction of *rac*-**1a** and **2x**, characteristic EPR signals corresponding to a phosphorus-centered radical adduct (**89**) were observed, with hyperfine coupling constants of (A_N = 14.0 G, A_H = 13.9 G, A_P = 37.1 G).[61,62] This radical species was further supported

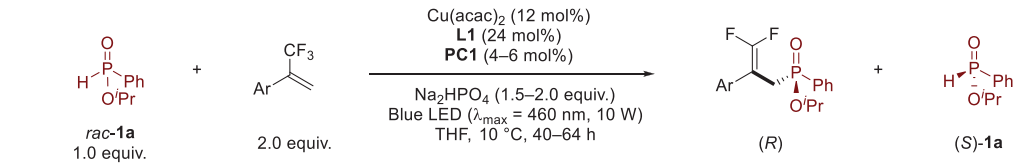

48 h	(*R*)-**26**	42% yield, 91% ee	(*S*)-**1a**	54% yield, 84% ee	*C* = 48%, *s* = 56
60 h	(*R*)-**14**	40% yield, 90% ee	(*S*)-**1a**	56% yield, 81% ee	*C* = 47%, *s* = 47
60 h	(*R*)-**27**	39% yield, 91% ee[a)]	(*S*)-**1a**	53% yield, 80% ee	*C* = 47%, *s* = 52
60 h	(*R*)-**29**	40% yield, 91% ee[a)]	(*S*)-**1a**	54% yield, 81% ee	*C* = 47%, *s* = 53
60 h	(*R*)-**31**	39% yield, 90% ee[a)]	(*S*)-**1a**	55% yield, 81% ee	*C* = 47%, *s* = 47
64 h	(*R*)-**35**	41% yield, 91% ee[a)]	(*S*)-**1a**	52% yield, 83% ee	*C* = 48%, *s* = 55
64 h	(*R*)-**41**	41% yield, 90% ee[a)]	(*S*)-**1a**	52% yield, 80% ee	*C* = 47%, *s* = 47
40 h	(*R*)-**13**	39% yield, 91% ee[a)]	(*S*)-**1a**	58% yield, 80% ee	*C* = 47%, *s* = 52
60 h	(*R*)-**15**	39% yield, 91% ee[a)]	(*S*)-**1a**	57% yield, 80% ee	*C* = 47%, *s* = 52
64 h	(*R*)-**28**	40% yield, 91% ee[a)]	(*S*)-**1a**	53% yield, 81% ee	*C* = 47%, *s* = 53
64 h	(*R*)-**30**	39% yield, 87% ee[a)]	(*S*)-**1a**	54% yield, 88% ee	*C* = 50%, *s* = 42
60 h	(*R*)-**32**	39% yield, 90% ee[a)]	(*S*)-**1a**	55% yield, 82% ee	*C* = 48%, *s* = 48
54 h	(*R*)-**39**	40% yield, 88% ee[a)]	(*S*)-**1a**	51% yield, 90% ee	*C* = 51%, *s* = 55
48 h	(*R*)-**47**	41% yield, 90% ee	(*S*)-**1a**	52% yield, 80% ee	*C* = 47%, *s* = 47

Scheme 4. Enhanced kinetic resolution for H-phosphinate recovery. Standard conditions: *rac*-**1a** (0.10 mmol), α-trifluoromethyl styrene derivatives (0.20 mmol), $Cu(acac)_2$ (0.012 mmol), **L1** (0.024 mmol), **PC1** (0.0040 mmol), Na_2HPO_4 (0.15 or 0.20 mmol), THF (1.0 mL), 10 °C, under argon. [a)] Using 0.0060 mmol of **PC1** rather than 0.0040 and 0.20 mmol of Na_2HPO_4. Calculated conversion (C) = $ee_s/(ee_s + ee_p)$. Selectivity factor (s) = $\ln[(1-C)(1-ee_s)]/\ln[(1-C)(1+ee_s)]$.

a) Radical trapping and EPR experiments

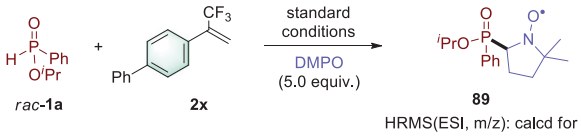

HRMS(ESI, m/z): calcd for $C_{15}H_{23}NO_3P^+$ $[M]^+$: 296.1416
found: 296.1413

• Standard reaction (DMPO trapping)

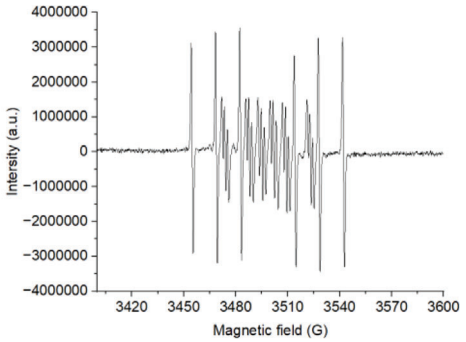

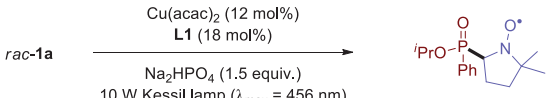

HRMS(ESI, m/z): calcd for $C_{15}H_{23}NO_3P^+$ $[M]^+$: 296.1416
found: 296.1411

• Reaction without **2x** and **PC1** (DMPO trapping)

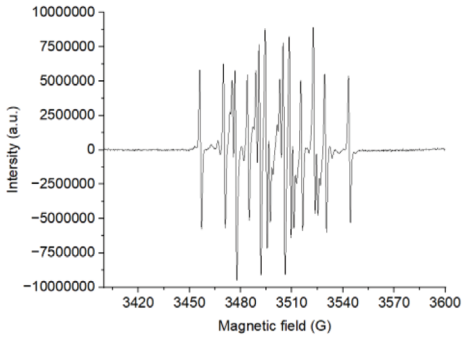

b) Additional evidence for P-centered radicals

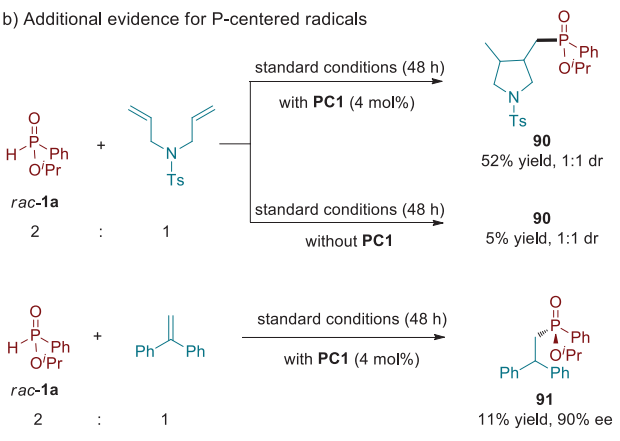

c) Stern-Volmer quenching experiments

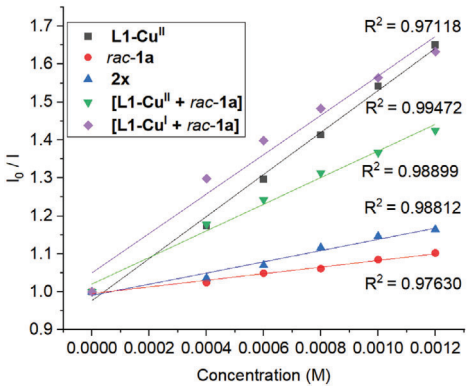

d) Non-linear effect experiments

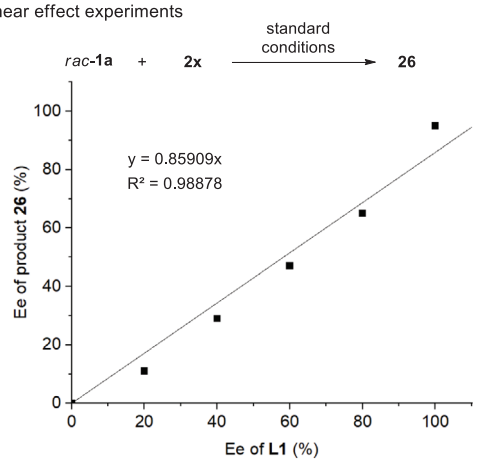

e) Kinetic resolution experiments

• Reaction in the presence of a chiral copper catalyst

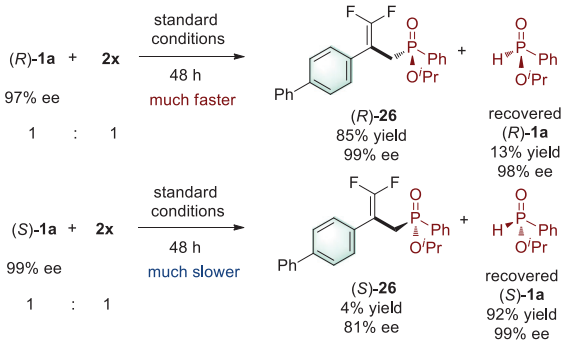

• Reaction in the presence of a racemic or achiral copper catalyst

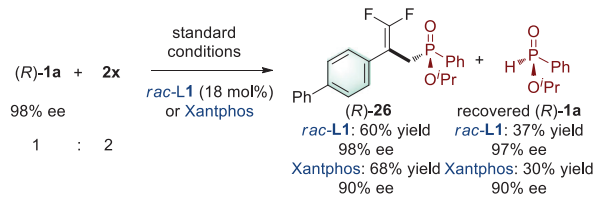

Scheme 5. Mechanistic studies.

by HRMS analysis (Scheme 5a). Notably, similar EPR signals (A_N = 14.0 G, A_H = 14.0 G, A_P = 37.2 G) were still detected when DMPO was added to a reaction system lacking both the α-trifluoromethyl styrene substrate (**2x**) and the photocatalyst 4CzIPN (**PC1**). However, these signals disappeared upon removal of light irradiation. The findings indicate that the generation of phosphorus-centered radicals is triggered by light irradiation and primarily depends on the H-phosphinate substrate and the copper catalyst, rather than the α-trifluoromethyl styrene substrate or the photocatalyst.

The reaction between *rac*-**1a** and *N*-tosyl diallylamine afforded a cyclized product (**90**) in 52% yield with a diastereomeric ratio (dr) of 1:1 (Scheme 5b). Interestingly, when the photocatalyst (**PC1**) was removed, the reaction still produced compound **90**, albeit at a significantly reduced yield (5%), and retained the same 1:1 dr. These results strongly support the proposed P-centered radical mechanism, indicating that phosphorus radicals can be generated via copper-induced photochemical processes, even in the absence of the photocatalyst.

Notably, the reaction of *rac*-**1a** with 1,1-diphenylethylene—a neutral olefin rather than an electron-deficient alkane—yielded the target product (**91**) in a modest yield (11%) but with exceptional enantioselectivity (90% ee). This outcome strengthens our hypothesis that stereoselective radical addition dominates over alternative pathways, such as nucleophilic addition of chiral copper phosphate species to electron-deficient alkenes. The contrasting reactivity toward neutral versus electron-deficient substrates further underscores the inherent stereocontrol of P-centered radicals, independent of substrate electronic effects.

Stern–Volmer quenching experiments were conducted to investigate potential interactions between the photocatalyst (**PC1**) and other reaction components (Scheme 5c). The results indicated that the excited state of the photocatalyst was more effectively quenched by copper species (**L1-Cu^{II}**, [**L1-Cu^{II}** + *rac*-**1a**], or [**L1-Cu^{I}** + *rac*-**1a**]) than by the substrates (*rac*-**1a**, **2x**).

Further mechanistic insights were obtained from non-linear effect studies in the reaction of *rac*-**1a** + **2x**→**26**, which revealed a direct linear correlation between the ee value of the chiral ligand (**L1**) and that of the product (**26**) (Scheme 5d).[63] This relationship substantiates the monomeric nature of the copper catalyst, which coordinates with a single chiral ligand, suggesting that a single catalyst species is responsible for asymmetric induction during C─P bond formation.

To investigate the stereochemical control of the kinetic resolution process, the two enantiomers of isopropyl phenylphosphinate (*rac*-**1a**) were separated via chiral HPLC chromatography, yielding (*R*)-**1a** (97% ee) and (*S*)-**1a** (99% ee). Each enantiomer was then subjected to the standard reaction with the α-trifluoromethyl styrene derivative (**2x**). Specifically, the reaction of (*R*)-**1a** (1.0 equiv.) with **2x** (1.0 equiv.) over 48 h yielded (*R*)-**26** in 85% yield with 99% ee, while recovering (*R*)-**1a** in a 13% yield with 98% ee. In contrast, the reaction of (*S*)-**1a** (1.0 equiv.) with **2x** (1.0 equiv.) for the same duration produced only 4% yield of (*S*)-**26** with 81% ee, and allowed the recovery of 92% of (*S*)-**1a** at 99% ee (Scheme 5e). These outcomes align well with the observed kinetic resolution efficiency, clearly demonstrating the system's capability to discriminate between the enantiomers of *rac*-**1a**.

Additionally, a reaction between (*R*)-**1a** (98% ee) and **2x** was carried out using a racemic copper catalyst ($Cu(acac)_2$ [12 mol%] + *rac*-**L1** [18 mol%]) and 4CzIPN (**PC1**, 0.0040 mmol) under standard conditions. Product **26** was obtained in 60% yield with 98% ee, while **1a** was recovered at 37% and with 97% ee. Moreover, a control experiment using the achiral ligand 9,9-dimethyl-4,5-bis(diphenylphosphino)xanthene (Xantphos) in place of *rac*-**L1** yielded both the product (90% ee) and recovered starting material (90% ee) with minimal erosion of enantiomeric excess, demonstrating that stereoretentive transformations occur independently of chiral ligand control. These results collectively support our hypothesis that the putative chiral metal-bound P-centered radical intermediate preferentially undergoes stereoretentive transformations over racemization, even in the presence of racemic or achiral ligands.

It is noteworthy that crude ^{1}H NMR analysis of the reaction between *rac*-**1a** and **2x**, conducted with either catalytic or stoichiometric amounts of the copper catalyst, showed no spectral signatures indicative of copper hydride intermediates. These findings imply that copper hydride-mediated pathways are unlikely to play a dominant role (see the Supporting Information for details).[64–67] Moreover, replacing 4CzIPN (**PC1**) with commonly employed energy transfer (EnT) catalysts, such as 9-fluorenone, thioxanthone, benzophenone anthracene, and Michler's ketone, resulted in no product formation, ruling out energy transfer processes as the primary mechanism (see the Supporting Information for details).[68,69]

Mechanistic Proposal

Building on our experimental outcomes and mechanistic investigations, we propose the following reaction pathways (Scheme 6a). The catalytic cycle commences with base-assisted ligand exchange between the copper catalyst and the H-phosphinate substrate (*rac*-**1a**), generating a chiral copper(II) intermediate (**INT-A**). Crucially, the chiral phosphine ligand exerts pronounced steric control at the metal center, inducing differential reactivity between substrate enantiomers. (*R*)-**1a** exhibits significantly accelerated reaction kinetics compared to its (*S*)-counterpart, thereby enabling efficient kinetic resolution. Subsequent photoinduced ligand-to-metal charge transfer (LMCT) triggers electronic reorganization, followed by oxygen-mediated rebinding to the metal center.[51,70,71] This sequence facilitates conversion of **INT-A** into a copper(I)-phosphorus radical intermediate (**INT-B**),[72–78] representing a critical transition in the catalytic cycle. Our mechanistic experiments, along with recent studies by Che et al., support that metal-bound P-centered radicals remain configurationally stable and do not undergo racemization under mild photochemical conditions.[79] Simultaneously, the photocatalyst (**PC1**) absorbs photons, transitioning to its excited state (**PC1***, $E_{1/2}^{red}$ (**PC1***/**PC1**$^{\bullet-}$) = 1.51 V),

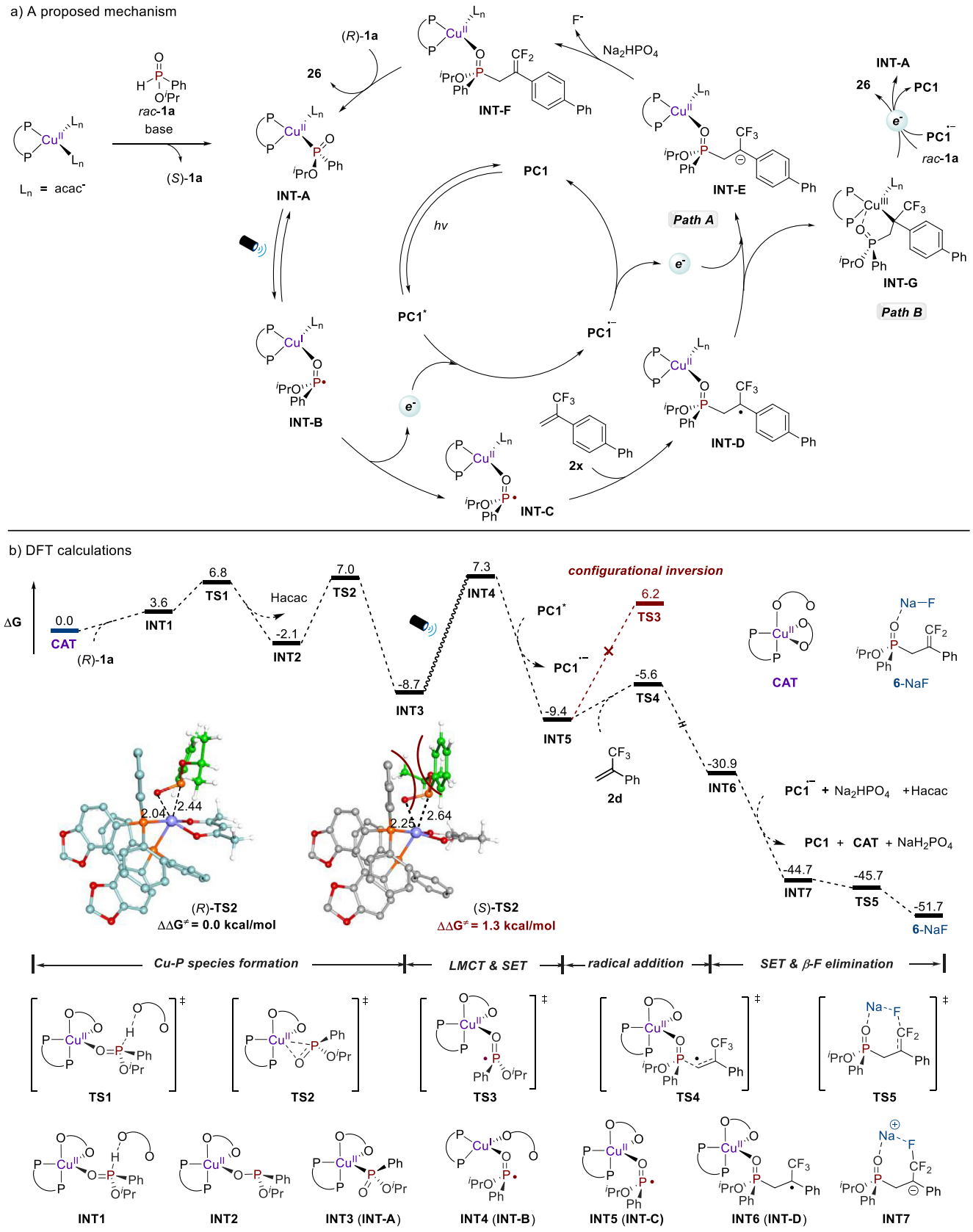

Scheme 6. Mechanism proposal and calculated energy profile of Cu-catalyzed reaction of (*R*)-**1a** with **2d**. DFT calculations were carried out using TPSSh/def2-TVZP/SMD(THF)//TPSSh/def2-SVP. Energies and bond distances are given in kcal mol^{-1} and Å, respectively.

which possesses sufficient redox potential to oxidize **INT-B** via single electron transfer (SET), yielding a copper(II)-phosphorus radical complex (**INT-C**).[43,80–84] **INT-C** then undergoes radical addition with the α-trifluoromethyl styrene substrate (**2x**), forming an alkyl radical complex (**INT-D**). Notably, an alternative pathway from intermediate **INT-B** to **INT-D** cannot be ruled out, wherein **INT-B** first adds to **2x**, followed by single electron transfer to generate **INT-D**.

Subsequently, single-electron reduction of **INT-D** by **PC1**$^{\bullet-}$ furnishes a carbon anion complex (**INT-E**), concomitantly regenerating the photocatalyst (**PC1**). Finally, β-fluorine elimination from **INT-E** produces a coordinated product (**INT-F**), which, after ligand exchange, affords the desired product (**26**). This process also regenerates the key intermediate (**INT-A**), enabling the next catalytic cycle (Path A). Alternatively, a copper-assisted β-fluorine elimination pathway involving alkyl-copper(III) species cannot be ruled out (Path B). Specifically, **INT-D** may undergo intermolecular radical capture to produce an alkyl-copper(III) intermediate (**INT-G**). Subsequent β-fluorine elimination from **INT-G**, coupled with single electron transfer from **PC1**$^{\bullet-}$ and ligand exchange with substrate *rac*-**1a** under basic conditions, delivers the target product (**26**) while regenerating the photocatalyst (**PC1**) and the key intermediate complex (**INT-A**). Both pathways are consistent with the experimental observations and provide a comprehensive mechanistic framework for the reaction.

Regarding the photochemical asymmetric C(sp^2)—P cross-coupling reaction between racemic H-phosphinates and vinyl fluorides, we believe that it proceeds through a similar sequence involving photoinduced P-centered radical formation, copper-mediated radical addition, single electron transfer, and ultimate β-fluorine elimination. This hypothesis is supported by preliminary experimental evidence, such as radical trapping studies (see the Supporting Information for details).

DFT Calculations

To gain deeper insights into the reaction process and the origins of stereodiscrimination, density functional theory (DFT) calculations were conducted (Scheme 6b). (*R*)-**1a** (the superior enantiomer) and **2d** were chosen as model substrates, utilizing one of the chiral diphosphines (**L2**) from our study as the ligand for computational analysis. The reaction begins with the active copper catalyst (**CAT**), where the reaction is initiated by ligand exchange between (*R*)-**1a** and acetylacetonate anion ($acac^-$), forming intermediate **INT1**. Subsequently, a proton transfer process occurs via transition state **TS1**, overcoming an energy barrier of 3.2 kcal mol^{-1} relative to **INT1**, yielding intermediate **INT2**. This intermediate then undergoes further transformation through a three-membered cyclic transition state (**TS2**, with a barrier of 9.1 kcal mol^{-1}) to generate the thermodynamically more stable intermediate **INT3** containing a Cu—P bond (corresponding to **INT-A** in the proposed mechanism).

INT3 undergoes a light-induced LMCT process accompanied by partial dissociation of an acac anion, producing a monovalent copper intermediate (**INT4**, corresponding to **INT-B**). **INT4** is subsequently oxidized by the excited-state photosensitizer **PC1**,[85] forming **INT5** (corresponding to **INT-C**)—a process calculated to be highly exergonic at 16.7 kcal mol^{-1}. The radical addition of **2d** then proceeds via transition state **TS4** (with a barrier of 3.8 kcal mol^{-1}), generating the *C*-centered radical (**INT6**, corresponding to **INT-D**) in a kinetically feasible manner. Notably, the configuration inversion of the phosphorus radical in **INT5** (via transition state **TS3**) requires overcoming a significantly higher energy barrier of 15.6 kcal mol^{-1} compared to the radical addition process (via **TS4**). This suggests that the radical addition process between the metal-bound phosphorus radical and the α-trifluoromethyl styrene substrate is predominant. Following this kinetic control, **INT6** is reduced by **PC1**$^{\bullet-}$ in the presence of Na_2HPO_4 and Hacac, forming a carbanion (**INT7**) and regenerating the active catalyst (**CAT**). Finally, the catalytic cycle is completed through Na^+-promoted β-fluoride elimination via transition state **TS5**, delivering the NaF-bonding product (**6**–NaF).[86] Overall, DFT calculations indicate that the entire reaction process is energetically favorable.

Furthermore, computational results reveal that the formation of the Cu—P species via a three-membered cyclic transition state represents both the rate-determining and enantio-determining step of the overall catalytic cycle. To elucidate the origin of enantioselectivity, stereoisomers of the critical transition state ((*R*)-**TS2** **versus** (*S*)-**TS2**) were analyzed. The results demonstrate that (*R*)-**TS2** is lower in energy than (*S*)-**TS2** by 1.3 kcal mol^{-1}, consistent with the experimentally observed enantioselectivity. Scrutiny of the optimized geometries indicates that the enantioselectivity is primarily attributed to stronger steric repulsion between the chiral ligand and the SPO moiety in (*S*)-**TS2** compared to (*R*)-**TS2**, leading to elongation of both Cu—O and Cu—P bonds between the copper center and the SPO moiety (2.25 versus 2.04 Å for Cu—O; 2.64 versus 2.44 Å for Cu—P), thus making (*S*)-**TS2** higher in energy than (*R*)-**TS2**.

Scale-Up Synthesis and Product Transformations

To demonstrate the practicality of our methodology, a scale-up synthesis of one *gem*-difluoroallylated P-chiral phosphinate product was performed (Scheme 7a). A solution containing isopropyl phenylphosphinate (*rac*-**1a**, 368.3 mg, 2.0 mmol), 4-(3,3,3-trifluoroprop-1-en-2-yl)-1,1′-biphenyl (**2x**, 124.1 mg, 0.50 mmol), 4CzIPN (**PC1**, 15.8 mg, 0.020 mmol), $Cu(acac)_2$ (15.7 mg, 0.060 mmol), **L1** (106.2 mg, 0.090 mmol), and Na_2HPO_4 (106.5 mg, 0.75 mmol) in THF (5.0 mL) was exposed to a 10 W Kessil lamp (λ_{max} = 456 nm) under standard conditions. The reaction afforded 158.3 mg of product **26** in a slightly reduced yield (77%) but with identical enantioselectivity (95% ee).

We further explored the synthetic versatility of compound **26** through various transformations. Treatment of **26** with TMSCN and Cs_2CO_3 in acetonitrile at room temperature for 24 h yielded the corresponding cyano-substituted derivative (**92**) value of 90%. Similarly, reacting **26** with benzimidazole in the presence of K_3PO_4 in DMF at ambient temperature

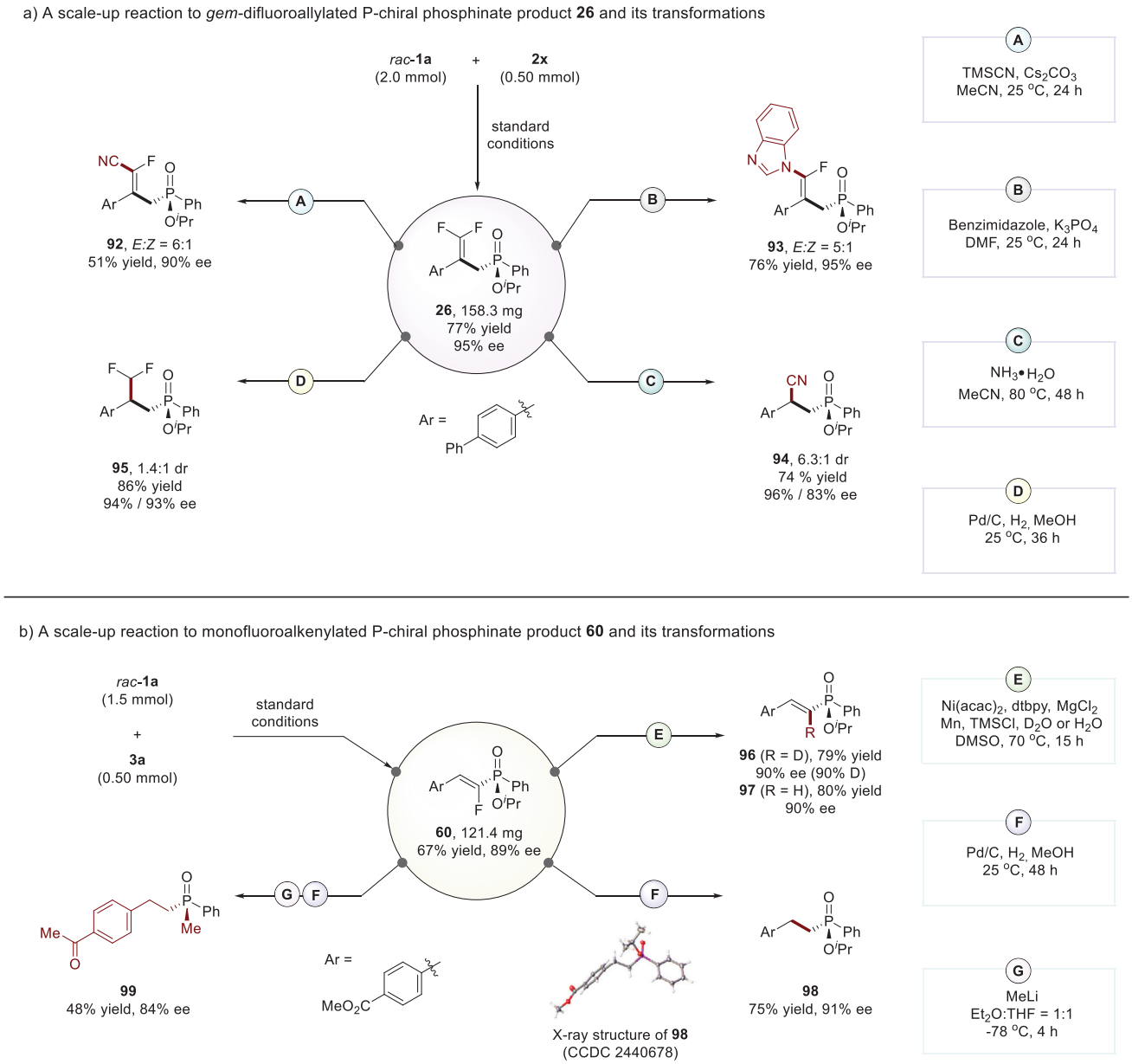

Scheme 7. Synthetic utility.

furnished product **93** in 76% yield and an excellent enantiomeric excess (95% ee), albeit with an *E:Z* ratio of 5:1. Additionally, when **26** was subjected to a sequential nucleophilic addition and double hydrogen fluoride elimination sequence using aqueous ammonia as both the nitrogen source for the "CN" functionality and as a base, the targeted α-aryl nitrile product (**94**) was obtained in a 74% yield, with 6.3:1 dr and 96% ee. Moreover, the difluoromethylene unit in **26** could be effectively converted into a difluoromethyl group via a Pd/C-catalyzed hydrogenation, affording product **95** in 86% yield with 1.4:1 dr and 94% ee.

The photochemical C(sp^2)—P cross-coupling reaction between *rac*-**1a** and methyl 4-(2,2-difluorovinyl)benzoate (**3a**) was also scalable (Scheme 7b). Product **60** (121.4 mg) was obtained in 67% yield and 89% ee, demonstrating consistent performance at larger scale. This compound served as a versatile intermediate for synthesizing various P-chiral derivatives with minimal loss of enantiomeric purity. For instance, selective defluorinative deuteration of **60** was achieved via a nickel-catalyzed reaction with D_2O in DMSO using $Ni(acac)_2$ as catalyst, 4,4′-di-*tert*-butyl-2,2′-bipyridine (dtbpy) as ligand, manganese powder as reductant, and magnesium chloride and TMSCl as additives, delivering deuterated P-chiral product (**96**) in 79% yield with 90% ee and 90% D-incorporation. Replacing D_2O with H_2O under the same conditions resulted in defluorinative hydrogenation producing the hydrogenated analog (**97**) in 80% yield with 90% ee. Catalytic hydrogenation of **60** using Pd/C enabled simultaneous defluorination and hydrogenation, yielding the P-alkylation product (**98**) in 75% yield with 91% ee. The structure of product **98** was

unambiguously determined by X-ray crystallographic analysis (CCDC No. 2440678).[56] Finally, treatment of **98** with MeLi generated a tertiary phosphine oxide (TPO) product (**99**) with a slight reduction in enantiomeric excess.

Conclusion

In summary, we have developed a paradigm-shifting strategy for stereocontrolled phosphorus radical chemistry, effectively addressing a long-standing challenge in asymmetric synthesis. By synergistically integrating a well-defined chiral diphosphine–copper catalyst with 4CzIPN-mediated photoredox catalysis, our platform merges kinetic resolution with light-driven generation of metal-bound P-centered radicals and their stereoretentive transformations. This approach enables unprecedented photochemical kinetic resolutions of racemic H-phosphinates using α-trifluoromethyl styrenes or *gem*-difluorostyrenes as coupling partners. A broad and structurally diverse array of fluorine-containing P-chiral phosphinates (85 examples)—compounds that are traditionally difficult to access yet of significant pharmaceutical relevance—were obtained with high enantioselectivity (up to 98% ee).

Mechanistic studies and DFT calculations reveal a three-stage stereochemical relay: 1) enantiodiscrimination of H-phosphinates by the chiral copper center, 2) photoinduced LMCT-driven generation of copper-bound P-radicals, and 3) stereoretentive C─P bond formation facilitated by the photoredox catalyst. This framework not only reconciles the inherent lability of P-centered radicals with precise stereocontrol but also establishes metallaphotoredox catalysis as a general solution for heteroatom-based asymmetric transformations where rapid configurational interconversion has historically hindered progress. The method's operational simplicity—utilizing air- and moisture-tolerant conditions, visible light activation, and noble-metal-free components—further underscores its synthetic appeal. Current efforts are focused on further improving stereochemical fidelity by temporally controlling reaction dynamics, leveraging advanced photocatalyst design and machine learning-assisted ligand optimization.

Acknowledgements

The authors gratefully acknowledge funding from the National Natural Science Foundation of China (No. 22371237, 22571265, 22571263), National Youth Talent Support Program, Fujian Provincial Natural Science Foundation of China (No. 2024J010002), and Open Research Fund of School of Chemistry and Chemical Engineering, Henan Normal University (No. 2024Y01).

Conflict of Interests

The authors declare no conflict of interest.

Data Availability Statement

The data that support the findings of this study are available in the Supporting Information of this article.

Keywords: Copper-photoredox catalysis · Kinetic resolution · P-chiral phosphinates · Phosphorus radical

[1] G. Bar, A. F. Parsons, *Chem. Soc. Rev.* **2003**, *32*, 251–263, https://doi.org/10.1039/b111414j.
[2] D. Leca, L. Fensterbank, E. Lacôte, M. Malacria, *Chem. Soc. Rev.* **2005**, *34*, 858–865, https://doi.org/10.1039/b500511f.
[3] G. G. Melikyan, *Acc. Chem. Res.* **2015**, *48*, 1065–1079, https://doi.org/10.1021/ar500365v.
[4] A. Studer, D. P. Curran, *Angew. Chem. Int. Ed.* **2016**, *55*, 58–102, https://doi.org/10.1002/anie.201505090.
[5] M. Yan, J. C. Lo, J. T. Edwards, P. S. Baran, *J. Am. Chem. Soc.* **2016**, *138*, 12692–12714, https://doi.org/10.1021/jacs.6b08856.
[6] J. M. Smith, S. J. Harwood, P. S. Baran, *Acc. Chem. Res.* **2018**, *51*, 1807–1817, https://doi.org/10.1021/acs.accounts.8b00209.
[7] D. Leifert, A. Studer, *Angew. Chem. Int. Ed.* **2020**, *59*, 74–108, https://doi.org/10.1002/anie.201903726.
[8] P.-Z. Wang, B. Zhang, W.-J. Xiao, J.-R. Chen, *Acc. Chem. Res.* **2024**, *57*, 3433–3448, https://doi.org/10.1021/acs.accounts.4c00638.
[9] J. J. A. Garwood, A. D. Chen, D. A. Nagib, *J. Am. Chem. Soc.* **2024**, *146*, 28034–28059.
[10] C. K. Prier, D. A. Rankic, D. W. C. MacMillan, *Chem. Rev.* **2013**, *113*, 5322–5363, https://doi.org/10.1021/cr300503r.
[11] D. A. Nagib, *Chem. Rev.* **2022**, *122*, 15989–15992, https://doi.org/10.1021/acs.chemrev.2c00622.
[12] C.-L. Wang, J. Wang, J.-K. Jin, B. Li, Y. L. Phang, F.-L. Zhang, T. Ye, H.-M. Xia, L.-W. Hui, J.-H. Su, Y. Fu, Y.-F. Wang, *Science* **2023**, *382*, 1056–1065, https://doi.org/10.1126/science.adg1322.
[13] A. M. Messinis, T. von Münchow, M. Surke, L. Ackermann, *Nat. Catal.* **2024**, *7*, 273–284, https://doi.org/10.1038/s41929-023-01105-0.
[14] Z. Zhu, X. Wu, Z. Li, D. A. Nicewicz, *Acc. Chem. Res.* **2025**, *58*, 1094–1108, https://doi.org/10.1021/acs.accounts.4c00837.
[15] X. Xin, J. Geng, D. Zhang, J.-A. Ma, J. Wu, *Nat. Synth.* **2024**, *4*, 177–187, https://doi.org/10.1038/s44160-024-00681-8.
[16] H. Wang, X. Gao, Z. Lv, T. Abdelilah, A. Lei, *Chem. Rev.* **2019**, *119*, 6769–6787, https://doi.org/10.1021/acs.chemrev.9b00045.
[17] L. F. T. Novaes, J. Liu, Y. Shen, L. Lu, J. M. Meinhardt, S. Lin, *Chem. Soc. Rev.* **2021**, *50*, 7941–8002, https://doi.org/10.1039/D1CS00223F.
[18] P. Melchiorre, *Chem. Rev.* **2022**, *122*, 1483–1484, https://doi.org/10.1021/acs.chemrev.1c00993.
[19] M. D. Palkowitz, M. A. Emmanuel, M. S. Oderinde, *Acc. Chem. Res.* **2023**, *56*, 2851–2865, https://doi.org/10.1021/acs.accounts.3c00479.
[20] L. Song, L. Cai, L. Gong, E. V. M. Van der Eycken, *Chem. Soc. Rev.* **2023**, *52*, 2358–2376, https://doi.org/10.1039/D2CS00734G.
[21] R. Suzuki, T. Ando, F. Deufel, K. Ohmatsu, T. Ooi, *Nat. Synth.* **2024**, *3*, 1385–1391, https://doi.org/10.1038/s44160-024-00612-7.
[22] Y. Dai, Y. Huang, Y. Wang, Y. Lin, Y. Liu, Q. Wei, X. Zhao, Y. Yin, Z. Jiang, *J. Am. Chem. Soc.* **2025**, *147*, 30499–30507, https://doi.org/10.1021/jacs.5c11656.
[23] A. J. Buckmelter, A. I. Kim, S. D. Rychnovsky, *J. Am. Chem. Soc.* **2000**, *122*, 9386–9390, https://doi.org/10.1021/ja002068k.
[24] M. J. Genzink, J. B. Kidd, W. B. Swords, T. P. Yoon, *Chem. Rev.* **2022**, *122*, 1654–1716, https://doi.org/10.1021/acs.chemrev.1c00467.

[25] S. Mondal, F. Dumur, D. Gigmes, M. P. Sibi, M. P. Bertrand, M. Nechab, *Chem. Rev.* **2022**, *122*, 5842–5976, https://doi.org/10.1021/acs.chemrev.1c00582.

[26] X.-Y. Dong, Z.-L. Li, Q.-S. Gu, X.-Y. Liu, *J. Am. Chem. Soc.* **2022**, *144*, 17319–17329, https://doi.org/10.1021/jacs.2c06718.

[27] J. S. Trimble, R. Crawshaw, F. J. Hardy, C. W. Levy, M. J. B. Brown, D. E. Fuerst, D. J. Heyes, R. Obexer, A. P. Green, *Nature* **2022**, *611*, 709–714, https://doi.org/10.1038/s41586-022-05335-3.

[28] N. Sun, J. Huang, J. Qian, T.-P. Zhou, J. Guo, L. Tang, W. Zhang, Y. Deng, W. Zhao, G. Wu, R.-Z. Liao, X. Chen, F. Zhong, Y. Wu, *Nature* **2022**, *611*, 715–720, https://doi.org/10.1038/s41586-022-05342-4.

[29] L. Cheng, D. Li, B. K. Mai, Z. Bo, L. Cheng, P. Liu, Y. Yang, *Science* **2023**, *381*, 444–451, https://doi.org/10.1126/science.adg2420.

[30] W.-C. C. Lee, X. P. Zhang, *Angew. Chem. Int. Ed.* **2024**, *63*, e202320243, https://doi.org/10.1002/anie.202320243.

[31] J. Sun, J. He, L. Massaro, D. A. Cagan, J. Tsien, Y. Wang, F. C. Attard, J. E. Smith, J. E. Lee, Y. Kawamata, P. S. Baran, *Nature* **2025**, *642*, 85–91, https://doi.org/10.1038/s41586-025-09011-0.

[32] Y.-F. Zhang, B. Wang, Z. Chen, J.-R. Liu, N.-Y. Yang, J.-M. Xiang, J. Liu, Q.-S. Gu, X. Hong, X.-Y. Liu, *Science* **2025**, *388*, 283–291, https://doi.org/10.1126/science.adu3996.

[33] V. Tseliou, L. Kqiku, M. Berger, F. Schiel, H. Zhou, G. J. Poelarends, P. Melchiorre, *Nature* **2024**, *634*, 848–854, https://doi.org/10.1038/s41586-024-08004-9.

[34] F. A. Kortmann, M.-C. Chang, E. Otten, E. P. A. Couzijn, M. Lutz, A. J. Minnaard, *Chem. Sci.* **2014**, *5*, 1322, https://doi.org/10.1039/c3sc52913d.

[35] W. G. Bentrude, E. R. Hansen, W. A. Khan, T. B. Min, P. E. Rogers, *J. Am. Chem. Soc.* **1973**, *95*, 2286–2293, https://doi.org/10.1021/ja00788a031.

[36] S. Lemouzy, L. Giordano, D. Hérault, G. Buono, *Eur. J. Org. Chem.* **2020**, *2020*, 3351–3366, https://doi.org/10.1002/ejoc.202000406.

[37] D. Gatineau, L. Giordano, G. Buono, *J. Am. Chem. Soc.* **2011**, *133*, 10728–10731, https://doi.org/10.1021/ja2034816.

[38] U. Pradere, E. C. Garnier-Amblard, S. J. Coats, F. Amblard, R. F. Schinazi, *Chem. Rev.* **2014**, *114*, 9154–9218, https://doi.org/10.1021/cr5002035.

[39] M. Dutartre, J. Bayardon, S. Jugé, *Chem. Soc. Rev.* **2016**, *45*, 5771–5794, https://doi.org/10.1039/C6CS00031B.

[40] S. K. Agrawal, S. Porey, Y. Bairagi, S. Maiti, A. C. Bissember, D. Maiti, *Chem. Soc. Rev.* **2025**, *54*, 6122–6174, https://doi.org/10.1039/D5CS00165J.

[41] M. J. Sofia, D. Bao, W. Chang, J. Du, D. Nagarathnam, S. Rachakonda, P. G. Reddy, B. S. Ross, P. Wang, H.-R. Zhang, S. Bansal, C. Espiritu, M. Keilman, A. M. Lam, H. M. M. Steuer, C. Niu, M. J. Otto, P. A. Furman, *J. Med. Chem.* **2010**, *53*, 7202–7218, https://doi.org/10.1021/jm100863x.

[42] K. C. Forbes, E. N. Jacobsen, *Science* **2022**, *376*, 1230–1236, https://doi.org/10.1126/science.abp8488.

[43] Y. Li, K. Zhou, Z. Wen, S. Cao, X. Shen, M. Lei, L. Gong, *J. Am. Chem. Soc.* **2018**, *140*, 15850–15858, https://doi.org/10.1021/jacs.8b09251.

[44] Y. Li, M. Lei, L. Gong, *Nat. Catal.* **2019**, *2*, 1016–1026, https://doi.org/10.1038/s41929-019-0357-9.

[45] B. Han, Y. Li, Y. Yu, L. Gong, *Nat. Commun.* **2019**, *10*, 3804, https://doi.org/10.1038/s41467-019-11688-7.

[46] S. Cao, W. Hong, Z. Ye, L. Gong, *Nat. Commun.* **2021**, *12*, 2377, https://doi.org/10.1038/s41467-021-22690-3.

[47] S. Cao, Z. Ye, Y. Chen, Y.-M. Lin, J. Fang, Y. Wang, B. Yang, L. Gong, *CCS Chem* **2022**, *4*, 3122–3133, https://doi.org/10.31635/ccschem.021.202101465.

[48] Z. Chi, J.-B. Liao, X. Cheng, Z. Ye, W. Yuan, Y.-M. Lin, L. Gong, *J. Am. Chem. Soc.* **2024**, *146*, 10857–10867, https://doi.org/10.1021/jacs.4c01443.

[49] F. Yang, L. Chi, Z. Ye, L. Gong, *J. Am. Chem. Soc.* **2025**, *147*, 1767–1780, https://doi.org/10.1021/jacs.4c13321.

[50] X. Cui, X. P. Zhang, *J. Am. Chem. Soc.* **2011**, *133*, 3304–3307, https://doi.org/10.1021/ja111334j.

[51] J. Li, Z. Zhang, L. Wu, W. Zhang, P. Chen, Z. Lin, G. Liu, *Nature* **2019**, *574*, 516–521, https://doi.org/10.1038/s41586-019-1655-8.

[52] P. Xu, J. Xie, D. Wang, X. P. Zhang, *Nat. Chem.* **2023**, *15*, 498–507, https://doi.org/10.1038/s41557-022-01119-4.

[53] M. Mendel, T. M. Karl, J. Hamm, S. J. Kaldas, T. Sperger, B. Mondal, F. Schoenebecket, *Nature* **2024**, *631*, 80–86, https://doi.org/10.1038/s41586-024-07555-1.

[54] F. Zhong, R. Li, B. K. Mai, P. Liu, G. C. Fu, *Nature* **2025**, *640*, 107–113, https://doi.org/10.1038/s41586-025-08784-8.

[55] H. Zhang, Y. Zhou, T. Yang, J. Wu, P. Chen, Z. Lin, G. Liu, *Nat. Catal.* **2025**, *8*, 58–66, https://doi.org/10.1038/s41929-024-01276-4.

[56] Deposition numbers 2361292 (for **27**), 2309605 (for **30**), 2440675 (for **60**) and 2440678 (for **98**) contain the supplementary crystallographic data for this paper. These data are provided free of charge by the joint Cambridge Crystallographic Data Centre and Fachinformationszentrum Karlsruhe Access Structures service via www.ccdc.cam.ac.uk/data_request/cif.

[57] Q. Dai, L. Liu, Y. Qian, W. Li, J. Zhang, *Angew. Chem. Int. Ed.* **2020**, *59*, 20645–20650, https://doi.org/10.1002/anie.202009358.

[58] C. Wang, X. Hu, C. Xu, Q. Ge, Q. Yang, J. Xiong, W.-L. Duan, *Angew. Chem. Int. Ed.* **2023**, *62*, e202300011.

[59] J. Zhang, J. Guo, R. Xu, D. Zheng, K. Lian, Z. Zhang, S. Cao, Z. Jiang, *Chem. Sci.* **2025**, *16*, 5957–5966, https://doi.org/10.1039/D5SC00358J.

[60] Z. Ye, Y. Yu, Y.-M. Lin, Y. Chen, S. Song, L. Gong, *Nat. Synth.* **2023**, *2*, 766–777, https://doi.org/10.1038/s44160-023-00291-w.

[61] G. R. Buettner, *Free Radical Biol. Med.* **1987**, *3*, 259–303, https://doi.org/10.1016/S0891-5849(87)80033-3.

[62] W.-Q. Liu, T. Lei, S. Zhou, X.-L. Yang, J. Li, B. Chen, J. Sivaguru, C.-H. Tung, L.-Z. Wu, *J. Am. Chem. Soc.* **2019**, *141*, 13941–13947, https://doi.org/10.1021/jacs.9b06920.

[63] T. Satyanarayana, S. Abraham, H. B. Kagan, *Angew. Chem. Int. Ed.* **2009**, *48*, 456–494, https://doi.org/10.1002/anie.200705241.

[64] H. Lv, Y. Cai, J. Zhang, *Angew. Chem. Int. Ed.* **2013**, *52*, 3203–3207, https://doi.org/10.1002/anie.201208364.

[65] S. D. Friis, M. T. Pirnot, L. N. Dupuis, S. L. Buchwald, *Angew. Chem. Int. Ed.* **2017**, *56*, 7242–7246, https://doi.org/10.1002/anie.201703400.

[66] T. Nakajima, Y. Kamiryo, K. Hachiken, K. Nakamae, Y. Ura, T. Tanase, *Inorg. Chem.* **2018**, *57*, 11005–11018, https://doi.org/10.1021/acs.inorgchem.8b01628.

[67] H. Sahoo, L. Zhang, J. Cheng, M. Nishiura, Z. Hou, *J. Am. Chem. Soc.* **2022**, *144*, 23585–23594, https://doi.org/10.1021/jacs.2c10754.

[68] G. Tan, M. Das, R. Kleinmans, F. Katzenburg, C. Daniliuc, F. Glorius, *Nat. Catal.* **2022**, *5*, 1120–1130, https://doi.org/10.1038/s41929-022-00883-3.

[69] R. Laskar, S. Dutta, J. C. Spies, P. Mukherjee, Á. Rentería-Gómez, R. E. Thielemann, C. G. Daniliuc, O. Gutierrez, F. Glorius, *J. Am. Chem. Soc.* **2024**, *146*, 10899–10907, https://doi.org/10.1021/jacs.4c01667.

[70] F. Juliá, *ChemCatChem.* **2022**, *14*, e202200916.

[71] S. M. Treacy, T. Rovis, *Synthesis* **2024**, *56*, 1967–1978.

[72] A. Hossain, A. Vidyasagar, C. Eichinger, C. Lankes, J. Phan, J. Rehbein, O. Reiser, *Angew. Chem. Int. Ed.* **2018**, *57*, 8288–8292, https://doi.org/10.1002/anie.201801678.

[73] W. Cheng, R. Shang, Y. Fu, *Nat. Commun.* **2018**, *9*, 5215, https://doi.org/10.1038/s41467-018-07694-w.

[74] S. I. Ting, S. Garakyaraghi, C. M. Taliaferro, B. J. Shields, G. D. Scholes, F. N. Castellano, A. G. Doyle, *J. Am. Chem. Soc.* **2020**, *142*, 5800–5810, https://doi.org/10.1021/jacs.0c00781.

[75] G. M. Torres, Y. Liu, B. A. Arndtsen, *Science* **2020**, *368*, 318–323, https://doi.org/10.1126/science.aba5901.
[76] Y.-C. Luo, F.-F. Tong, Y. Zhang, C.-Y. He, X. Zhang, *J. Am. Chem. Soc.* **2021**, *143*, 13971–13979, https://doi.org/10.1021/jacs.1c07459.
[77] S. Sarkar, K. P. S. Cheung, V. Gevorgyan, *Angew. Chem. Int. Ed.* **2024**, *63*, e202311972.
[78] N. Oku, R. Saeki, Y. Doi, K. Yamazaki, T. Miura, *Org. Lett.* **2025**, *27*, 3361–3367, https://doi.org/10.1021/acs.orglett.5c00761.
[79] Y. Zhang, J. Yuan, G. Huang, H. Yu, J. Liu, J. Chen, S. Meng, J.-J. Zhong, L. Dang, G.-A. Yu, C.-M. Che, *Chem. Sci.* **2022**, *13*, 6519–6524, https://doi.org/10.1039/D2SC00036A.
[80] R. Qi, C. Wang, Y. Huo, H. Chai, H. Wang, Z. Ma, L. Liu, R. Wang, Z. Xu, *J. Am. Chem. Soc.* **2021**, *143*, 12777–12783, https://doi.org/10.1021/jacs.1c05890.
[81] Q. Li, S. N. Gockel, G. A. Lutovsky, K. S. DeGlopper, N. J. Baldwin, M. W. Bundesmann, J. W. Tucker, S. W. Bagley, T. P. Yoon, *Nat. Chem.* **2022**, *14*, 94–99, https://doi.org/10.1038/s41557-021-00834-8.
[82] C. Chen, G. C. Fu, *Nature* **2023**, *618*, 301–307, https://doi.org/10.1038/s41586-023-06001-y.
[83] N. W. Dow, P. S. Pedersen, T. Q. Chen, D. C. Blakemore, A.-M. Dechert-Schmitt, T. Knauber, D. W. C. MacMillan, *J. Am. Chem. Soc.* **2022**, *144*, 6163–6172, https://doi.org/10.1021/jacs.2c01630.
[84] H. Lee, J. M. Ahn, P. H. Oyala, C. Citek, H. Yin, G. C. Fu, J. C. Peters, *J. Am. Chem. Soc.* **2022**, *144*, 4114–4123, https://doi.org/10.1021/jacs.1c13151.
[85] Y. Wu, J. Kang, H. Zhu, M. Bi, J. Li, Q. Meng, X. Lyu, Z. Wu, *ACS Sustainable Chem. Eng.* **2024**, *12*, 6640–6647, https://doi.org/10.1021/acssuschemeng.4c00202.
[86] T. Yao, C. Zhao, C. Li, Q. Song, *Org. Lett.* **2025**, *27*, 2597–2601, https://doi.org/10.1021/acs.orglett.5c00259.

Manuscript received: September 25, 2025
Revised manuscript received: November 11, 2025
Manuscript accepted: November 11, 2025
Version of record online: ■■, ■■